AGU ADVANCING EARTH AND SPACE SCIENCES

Geophysical Research Letters

RESEARCH LETTER
10.1029/2024GL111071

Optimising Interannual Sea Ice Thickness Variability Retrieved From CryoSat-2

Carmen Nab[1,2], Robbie Mallett[1,3,4], Connor Nelson[1], Julienne Stroeve[1,4,5], and Michel Tsamados[1]

[1]Centre for Polar Observation and Modelling, Department of Earth Sciences, University College London, London, UK, [2]Ocean Forecasting Research & Development, Met Office, Exeter, UK, [3]Earth Observation Group, Department of Physics and Technology, UiT the Arctic University of Norway, Tromsø, Norway, [4]Centre for Earth Observation Science, Clayton H. Riddell Faculty of Environment, Earth and Resources, University of Manitoba, Winnipeg, MB, Canada, [5]National Snow and Ice Data Center, University of Colorado Boulder, Boulder, CO, USA

Abstract Satellite radar altimeters like CryoSat-2 estimate sea ice thickness by measuring the return-time of transmitted radar pulses, reflected from the sea ice and ocean surface, to measure the radar freeboard. Converting freeboard to thickness requires an assumption regarding the fractional depth of the snowpack from which the radar waves backscatter (α). We derive sea ice thickness from CryoSat-2 radar freeboard data with incremental values for α, for the 2010–2021 winter periods. By comparing these to sea ice thickness estimates derived from upward-looking sonar moorings, we find that α values between 35%–80% result in the best representation of interannual variability observed over first-year ice, reduced to <55% over multi-year ice. The underestimating bias in retrievals caused by optimizing this metric can be removed by reducing the waveform retracking threshold to 20%–50%. Our results pave the way for a new generation of 'partial penetration' sea ice thickness products from radar altimeters.

Plain Language Summary Satellite altimeters like CryoSat-2 can be used to estimate sea ice thickness by estimating how far sea ice floes stick out above the waterline. This is done by measuring the time taken for radar waves to travel to the surface of the ice floe and back to the altimeter. All current winter sea ice thickness estimates assume that the radar waves return entirely from the sea ice surface, and not from the overlying snow cover. A growing body of research suggests this may not be the case, with weather and snow conditions affecting the fraction of the detected radar power that comes from the ice surface. We consider how well CryoSat-2 estimates capture whether the ice is thicker or thinner than usual at a given time of year. We find that its skill is highest when we assume that 35%–80% of the radar power comes from the sea ice surface, and 20%–65% comes from the snow surface. However, improving this aspect of skill makes the sea ice thickness estimates too low. To address this, we show that a simple change in the waveform processing method can counter this bias.

Key Points:

- CryoSat-2 retrievals of sea ice thickness have historically been tuned to minimize bias rather than to capture interannual variability
- We use upward-looking sonar moorings to tune the treatment of both waveform retracking and snowpack penetration by radar waves
- Tuning to optimize interannual variability indicates partial penetration for all retracking thresholds

Supporting Information:

Supporting Information may be found in the online version of this article.

Correspondence to:

C. Nab,
carmen.nab.18@ucl.ac.uk

Citation:

Nab, C., Mallett, R., Nelson, C., Stroeve, J., & Tsamados, M. (2024). Optimising interannual sea ice thickness variability retrieved from CryoSat-2. *Geophysical Research Letters*, *51*, e2024GL111071. https://doi.org/10.1029/2024GL111071

Received 27 JUN 2024
Accepted 18 OCT 2024

Author Contributions:

Conceptualization: Robbie Mallett
Data curation: Carmen Nab, Connor Nelson
Formal analysis: Carmen Nab, Robbie Mallett
Investigation: Carmen Nab, Robbie Mallett
Writing – original draft: Carmen Nab, Robbie Mallett
Writing – review & editing: Carmen Nab, Robbie Mallett, Julienne Stroeve, Michel Tsamados

1. Introduction

The Arctic's sea ice cover is decreasing in extent, age and thickness (Kwok, 2018; Stroeve & Notz, 2018) as the region warms at nearly four times the global average rate (Rantanen et al., 2022). Accurate monitoring of Arctic sea ice thickness is vital to understanding regional climate change, and the impact of that change on Arctic communities, shipping routes, and wildlife living on and under the ice (e.g., Howell et al., 2024; Stroeve et al., 2024).

Sea ice thickness can be estimated using satellite radar altimeters such as CryoSat-2, by estimating the range between the sea ice surface and the altimeter. The same can then be done for the nearby ocean surface, with the difference between these two measurements of radar range referred to as the *radar freeboard*. Using assumptions of hydrostatic equilibrium, snow depth and sea ice and snow density, sea ice thickness can then be calculated (e.g., Laxon et al., 2003). Studies have shown that the largest contributions to radar altimeter-derived sea ice thickness bias come from the snow basal salinity, sea ice roughness and partial snow penetration of the radar pulses (e.g., Landy et al., 2020; Ricker et al., 2014).

The radar range to the top of a sea ice floe is calculated through analysis of returned radar waveforms. Specifically, the waveforms are *retracked* to obtain the range to a presumed mean scattering height within the radar footprint, with the choice of retracking algorithm affecting the range retrieved. The most commonly used retracking approach is the threshold-first-maximum algorithm (TFMRA), which applies a fixed percentage threshold to the waveform's first maximum power return (e.g., Laxon et al., 2003; Ricker et al., 2014). Converting radar freeboard to sea ice thickness then requires an assumed value for the fractional depth of the snowpack from which the radar returns backscatter (α). We point out that the issue at hand is where returned radar waves backscatter from, rather than where they penetrate to, since they may be absorbed or scattered without returning. An assumption of $\alpha = 1$ implies that received radar waves are backscattered from a mean range corresponding to the base of the snowpack (the top of the sea ice). Assuming $0 < \alpha < 1$ corresponds to an assumed mean backscattering height within the snowpack. An example of this would be where a fraction of the radar waves is backscattered from the top of the snow and the remaining fraction is backscattered from the top of the sea ice.

A growing body of research now indicates that α is not consistent under all meteorological and snow physical conditions. Theoretical studies by Nandan et al. (2017, 2020) have indicated that snow salinity may play a key role in reducing the ability of CryoSat-2's radar waves to reach the sea ice surface. Surface-based studies document a strong backscattering response from ranges above the ice surface (e.g., Willatt et al., 2010, 2023), implying low α values. However, it has been suggested that the ice surface may be less specular relative to the snow surface at the viewing geometry and length scale of a surface-based instrument, suppressing its visibility to those instruments (De Rijke-Thomas et al., 2023). Airborne investigations such as those by Willatt et al. (2011) and King et al. (2018) also imply that Ku-band radar waves do not always return from the base of the snowpack. The airborne investigation by De Rijke-Thomas et al. (2023) found that although most power did return from the snow-ice interface over landfast first-year ice (FYI), the air-snow interface provided stronger backscatter for around 30% of returns.

Given the potential sensitivity of α derivations to the altitude and viewing geometry of the investigating instrument, satellite-based approaches to the question of CryoSat-2's α values are particularly desirable. Ricker et al. (2015) found that snowfall at drifting buoys led to increases in CryoSat-2's radar freeboards, contrary to the expected decrease if $\alpha = 1$. Nab et al. (2023) examined pan-Arctic changes in radar freeboard in response to snow accumulation from a reanalysis-driven model, and found that it also increased with accumulation. The authors derived a mean α value of ~ 0.6. However, both Ricker et al. (2015) and Nab et al. (2023) examined the sensitivity of radar freeboards on short timescales: This leaves open the possiblity that snowfall events are associated with temporary suppression of α (for instance due to changing the roughness of the surface), with α otherwise being very high. In this paper, we present a new method for calculating α that is not constrained to synoptic timescales.

Despite previous findings, all current winter sea ice thickness estimates using Cryosat-2 rely on the assumption that all returned Ku-band radar waves have fully penetrated the snowpack and backscattered from the sea ice surface ($\alpha = 1$). Despite this, thickness retrievals generally have a low bias compared to independent observations, due to what could be described as tuning: Competing biases in the sea ice thickness processing chain cancel out to give an appropriate final value, at the cost of intermediate values (such as the radar freeboard) having limited physical meaning. Here, we argue that instead of tuning our processing chains to the absolute sea ice thickness values themselves, we should also consider optimizing the interannual variability in sea ice thickness. This is because knowledge of whether the sea ice is thicker or thinner than usual in a given year is often critical for operational uses, and is also a key aspect of trend and regime-shift detection. We will also go on to show that tuning to interannual variability offers a unique optimum combination of retracker-threshold and penetration-values, whereas tuning to bias does not.

We first reflect on the conventional method of evaluation for CryoSat-2 derived sea ice thickness products at upward-looking sonar moorings. We then introduce our new method of evaluating sea ice thickness products based on their ability to capture interannual variability, and present an example application of this method. We do this by creating an ensemble of sea ice thickness estimates with incremental combinations of α and TFMRA threshold, assessing the skill of each member at the moorings relative to both bias and interannual variability.

2. Data

2.1. Sea Ice Thickness From Upward-Looking Sonar Moorings

Sea ice thickness is derived from bottom-anchored moorings equipped with upward-looking sonars, which estimate sea ice draft continuously at two-second intervals. In this paper we use mooring data collected by the Beaufort Gyre Exploration Project (BGEP) and at the Fram Strait Arctic Outflow Observatory (AOO). The AOO data used here was collected at four locations (F11–F14) from 2010–2019 (Sumata et al., 2022), while the BGEP data was collected at three locations (BGEP-A, BGEP-B and BGEP-D) from 2010–2021 (BGEP, 2022). The location and active period of the moorings are shown in Figure S1 in Supporting Information S1. We convert draft measurements from both campaigns into monthly averages, and then derive sea ice freeboard as per Equation 2 of S. Kern et al. (2015):

$$F_i = \frac{D(\rho_w - \rho_i) - h_s\rho_s}{\rho_i} \tag{1}$$

where D is monthly sea ice draft, ρ_w is the density of seawater (1,023.9 kgm^{-3}), h_s is the snow depth, ρ_s is the snow density and ρ_i is the bulk density of sea ice. The sea ice type product of Aaboe et al. (2021) is used to classify measurement as FYI or multi-year ice (MYI). Sea ice bulk densities of 916.7 and 882 kgm^{-3} are used for FYI and MYI, respectively, per Alexandrov et al. (2010). For snow depth and snow density, daily estimates from SnowModel-LG are used (ERA-5 version; Liston et al., 2020, 2021). SIT is then calculated from the ice freeboard assuming hydrostatic equilibrium:

$$SIT = \frac{F_i\rho_w + h_s\rho_s}{\rho_w - \rho_i} \tag{2}$$

Due to their close proximity (<50 km apart), we make a single timeseries of monthly SIT averages for the AOO moorings.

The mooring data shows clear interannual variability, with mean monthly sea ice thickness values ranging from 0–1.97 m in October (mean 0.65 m) and 0.95–2.34 m in April (mean 1.8 m).

2.2. CryoSat-2 Monthly Sea Ice Thickness

Next, we create monthly sea ice thickness products for all CryoSat-2 radar freeboard tracks that pass within 25 km of any of the seven moorings during the 2010–2021 winter season period (October–April). We do this by processing CryoSat-2 waveforms (Level 1B, Baseline D) using the pysiral package (Hendricks et al., 2024).

The waveform retracking and subsequent radar freeboard estimates were carried out using pysiral following the AWI CS2 L2 v2.6 near real time processing chain (Hendricks & Paul, 2023), with two exceptions: (a) We processed the sea ice waveforms using retracking thresholds of 5%–95%, increasing in increments of 2.5%, whilst keeping the threshold used to process lead waveforms at 50%. (b) We used the OSI SAF (2022) sea ice concentration product for surface classification, rather than the OSI SAF operational product.

The resulting radar freeboards within a 25 km radius of each mooring are then averaged to produce a monthly radar freeboard product at each mooring.

The radar freeboards (F_r) are then converted to sea ice freeboard (F_i) as per Equation 6.1 of Lawrence (2019):

$$F_i = F_r + \left(\alpha\frac{c}{c_s} - 1\right)h_s \tag{3}$$

where α is the fractional depth of the snowpack from which the radar waves backscatter, c is the speed of light in air (3.0×10^8 ms^{-1}) and c_s is the speed of light in snow (2.4×10^8 ms^{-1} in this study). We calculate sea ice freeboard using α values between 0 and 1, increasing in increments of 0.01. Assuming hydrostatic equilibrium, SIT is then computed as per Equation 2. The values for ρ_w, ρ_s, ρ_i and h_s used are the same as those used in Section 2.1.

3. Methods and Results

3.1. Reassessing the Skill of Publicly Available Monthly Products

We begin by reflecting on the conventional metric for the skill of CryoSat-2 derived sea ice thickness products: This might be referred to as the 'all-months correlation analysis'. A typical version of this analysis is shown in Figure 1a: The sea ice thickness in all winter months are scatter-plotted against the coincident sea ice thickness derived at upward-looking sonar moorings; R^2 and Root Mean Square Error (RMSE) values are generally calculated from the plot. Versions of this plot and analysis appear in Laxon et al. (2013); Kwok and Cunningham (2015); Guerreiro et al. (2017); Tilling et al. (2018); Jiang et al. (2023); Bocquet et al. (2023). Climatologically high ice thickness values in April generally inhabit the top-right hand corner of these plots, and climatologically lower sea ice thickness values from October generally inhabit the bottom left area. This consistent pattern results in generally high R^2 correlation values in excess of 0.6.

To meaningfully assess the skill of publicly available monthly sea ice thickness products, we compare their skill against that of their monthly climatologies in the all-months correlation analysis. To do this we download three publicly available monthly sea ice thickness products from the Goddard Space Flight Center (GSFC; Kurtz et al., 2014), the Center for Polar Observation and Modeling (CPOM; Tilling et al., 2018) and the Alfred Wegener Institute (AWI; Hendricks & Paul, 2023). We then construct a monthly climatology for each product over the 2010–2021 winter season period (October–April): These contain no information about whether the sea ice is thicker or thinner than usual in a given year. We characterize the skill of each publicly available product and its derived climatology with the conventional 'all-months correlation analysis'.

It transpires that the R^2 value for each of the products is lower than that of its climatology, which contains no representation of interannual variability. While R^2 skills are generally high (>0.6), the skills of the climatologies, which contain no information about a given year's radar data, are higher. This is because the seasonal cycle of sea ice thickening at the moorings and in satellite products is highly predictable: April thicknesses are consistently much higher than October thicknesses in both products, which produces high R^2 values. We performed this analysis by averaging CryoSat-2 retrievals within 100 km of a given mooring. We observed the real products to fare less well against their climatologies when the analysis was conducted with smaller radii (25 and 50 km; Figures S2 and S3 in Supporting Information S1), with the exception of the AWI product at a 50 km radius, which marginally outperforms its climatology.

When replicating the analysis in Figure 1 for a single month, we find markedly reduced R^2 values, because the products struggle to capture interannual variability (as opposed to the seasonal cycle). This impairment becomes stronger over the winter. For instance, when the analysis is performed just for January, the R^2 values for the AWI, CPOM and GSFC products are reduced to 0.45, 0.21 and 0.31 respectively (Figure S4 in Supporting Information S1). By April, these values are 0.22, 0.14 and 0.10 (Figure S5 in Supporting Information S1). A full table of R^2 and RMSE values is given in Table S1 in Supporting Information S1. While the R^2 values are reduced when only a single month is considered, the 'real' products do now significantly outperform their climatologies. We suggest that the degree of this outperformance is a good metric of a product's skill. These results show that neither the R^2 or RMSE metrics in the conventional analysis (shown on the left of Figure 1) are apt for capturing a product's skill in representing the sea ice thickness *anomaly* from what it typically is at that time of year.

3.2. Optimizing Retracking Threshold and Assumed Radar Penetration

Before investigating the effect of adjusting the TFMRA thresholds away from those traditionally used, we briefly summarize how this might be justified. We first note that the AWI threshold of 50% is entirely empirically motivated, based on the bias-minimization approach of Ricker et al. (2014) using $\alpha = 1$. We suggest that the use of a lower α value would have motivated a lower threshold. The CPOM threshold of 70% is not empirically motivated by a similar sensitivity analysis, but instead by the theoretical impulse response of a SAR radar over a surface with Gaussian roughness statistics (see Equation 2.4 and Figure 2.4 of Tilling, 2016). A substantial body of research now indicates that sea ice surfaces are better described by a non-symmetrical roughness distribution

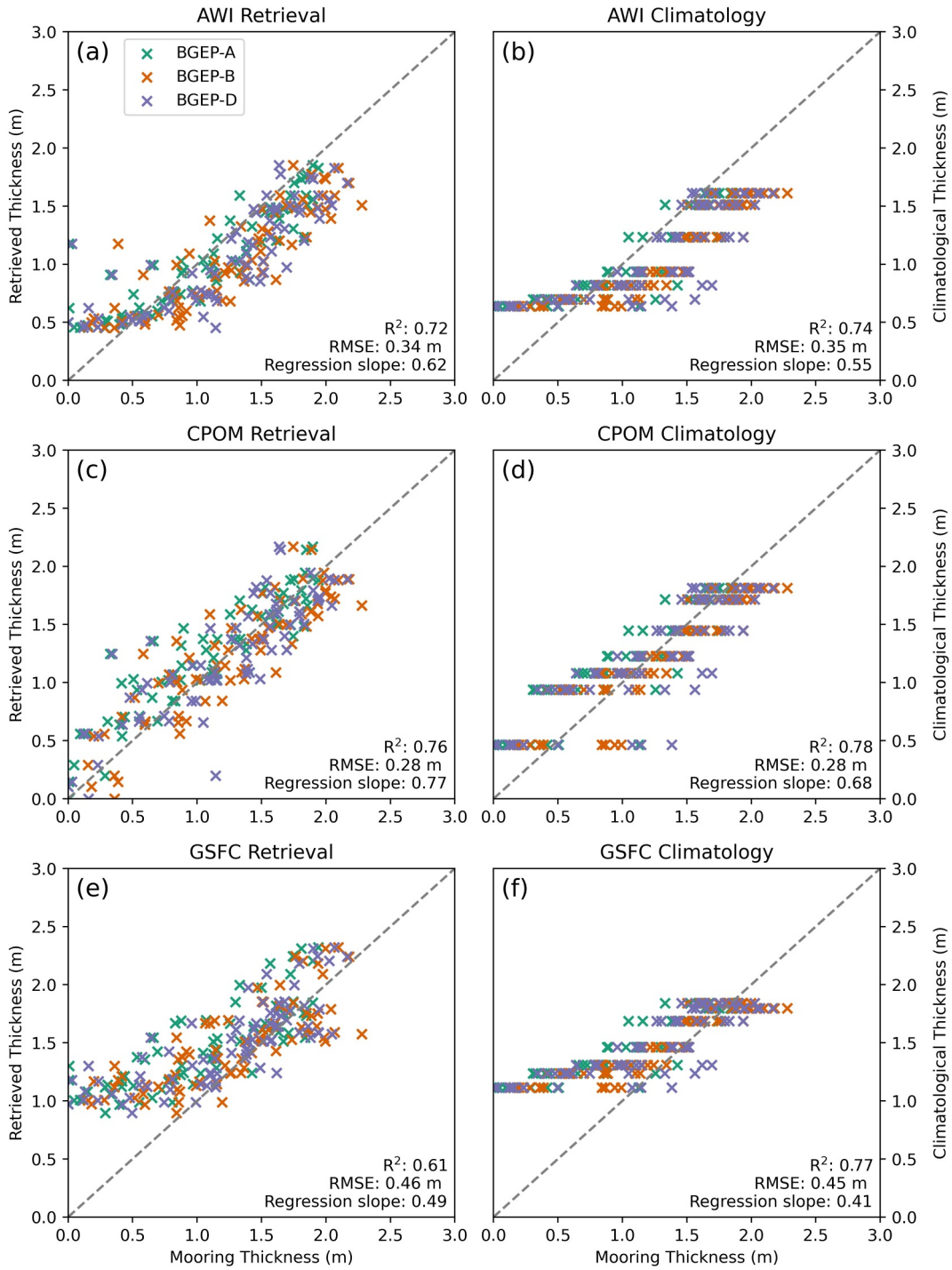

Figure 1. Publicly available monthly SIT products compared to their climatologies, for grid cells within 100 km of at least one of the BGEP moorings. The AOO moorings are exluded from this analysis, as none of the publicly available monthly SIT products include data in the Fram Strait region. Left-hand plots represent those traditionally presented in evaluation exercises, right hand plots indicate the performance of each product's climatology. We note that none of the SIT products outperform their climatologies at this radius.

(e.g., Landy et al., 2020), the skewness of which affects the appropriate retracking threshold. We therefore consider it justified to suggest empirical adjustments to the retracking threshold in order to minimize bias, following the approach of Ricker et al. (2014).

For each combination of α and TFMRA threshold, we thus calculate interannual skill statistics by producing a climatology for each of our sea ice thickness products at each mooring. This yields the average sea ice thickness for each winter month at each mooring. We then calculate the bias between the CryoSat-2 SIT values and mooring SIT values by considering the average difference in the values at each α and retracking threshold combination. This is done for all moorings, and also separately for the AOO and BGEP clusters. This produces a single mean bias value for each combination (Figure 2, left column).

We find the lowest mean bias values ($\leq$0.8 m) along a line which runs between threshold values of 20%–50%, depending on the α value (Figure 2, left column). The minimum mean biases, shown by the black lines in Figure 2, were found to be <0.17 m and <0.12 m for the AOO and BGEP moorings, respectively, although this may be further reducible by varying the retracking thresholds at smaller increments. Tuning to the lowest mean bias in sea ice thickness products is therefore possible at every tested value of assumed radar penetration, as any bias induced by assuming partial penetration can be counter-acted by choosing the most appropriate retracking threshold. This makes clear that the best combination of threshold and assumed radar penetration values cannot be found with analysis of bias alone. We should therefore also consider the CS2-derived products' ability to represent the interannual variability measured at the moorings.

To evaluate each combination's skill at capturing interannual variability, we create a list of anomalies from the climatology for each winter month, for each mooring, over the 2010–2021 period. We then calculate the RMSE between the CryoSat-2-based anomalies and the analogous anomalies calculated from the mooring-derived sea ice thickness data, again for all moorings but also for the separate clusters (Figure 2, right-hand column). Examples of the resulting scatterplots for individual combinations can be found in Figure S6 in Supporting Information S1. We find the lowest RMSEs (0.35–0.4 m) at retracking thresholds of 70%–85% and $0.4 < \alpha < 0.75$ when combining the two mooring datasets (Figure 2f). Overall, for the separate and combined mooring datasets, the optimal α is never 1, at any given threshold. We also calculate the linear correlation coefficient between the CS2- and mooring-derived SIT anomalies at each threshold and α combination, but find this metric inferior to the RMSE as it does not capture the slope between the two datasets, such that the linear correlation coefficient and slope have to be considered together to find the optimal combination. This analysis is shown in Section 1 in Supporting Information S1, and results in similar optimal α values to the RMSE analysis (Figures S7 and S8 in Supporting Information S1).

Our analysis of the two skill metrics (bias and interannual variability) reveals a tension between them. It appears that, although there are many combinations of α and TFMRA value that effectively minimize bias, none of them lie where retrievals are most skillful at capturing variability. This points to the presence of other, untested biases in the retrieval chain which we will discuss in Section 4.

3.3. Ice Type Dependence of α

We note that there is a higher prevalence of FYI (69% and 80% of data points for BGEP and AOO, respectively) than MYI at the moorings during the time period analyzed in this study. To determine whether there is an ice type dependence in our calculated values, we calculate the optimal α and retracking threshold over each ice type separately.

We find a clear difference in the optimal α and retracking threshold combinations over first-year and MYI (Figure 3). Over FYI, the lowest RMSEs are found at thresholds of 60%–85% when assuming $0.35 < \alpha < 0.8$, compared to 50%–75% and $0.25 < \alpha < 0.55$ over MYI. Lower RMSEs were found over FYI than MYI, with minimum mean biases (shown by the black lines in Figure 3) of <0.18 m and <0.13 m, respectively. This illustrates the potential benefits of having ice type dependent TFMRA threshold and α values.

4. Discussion and Conclusions

4.1. Snow and Ice Property Dependence of α

It is striking that the interannual skill of our CryoSat-2 retrievals is higher in general over MYI. Retrievals over MYI are considerably more skillful for any value of α than for even the optimal α value for FYI. This might be explained by the higher freeboards associated with MYI, which are more easily discerned by CryoSat-2 (Ricker et al., 2017).

10.1029/2024GL111071

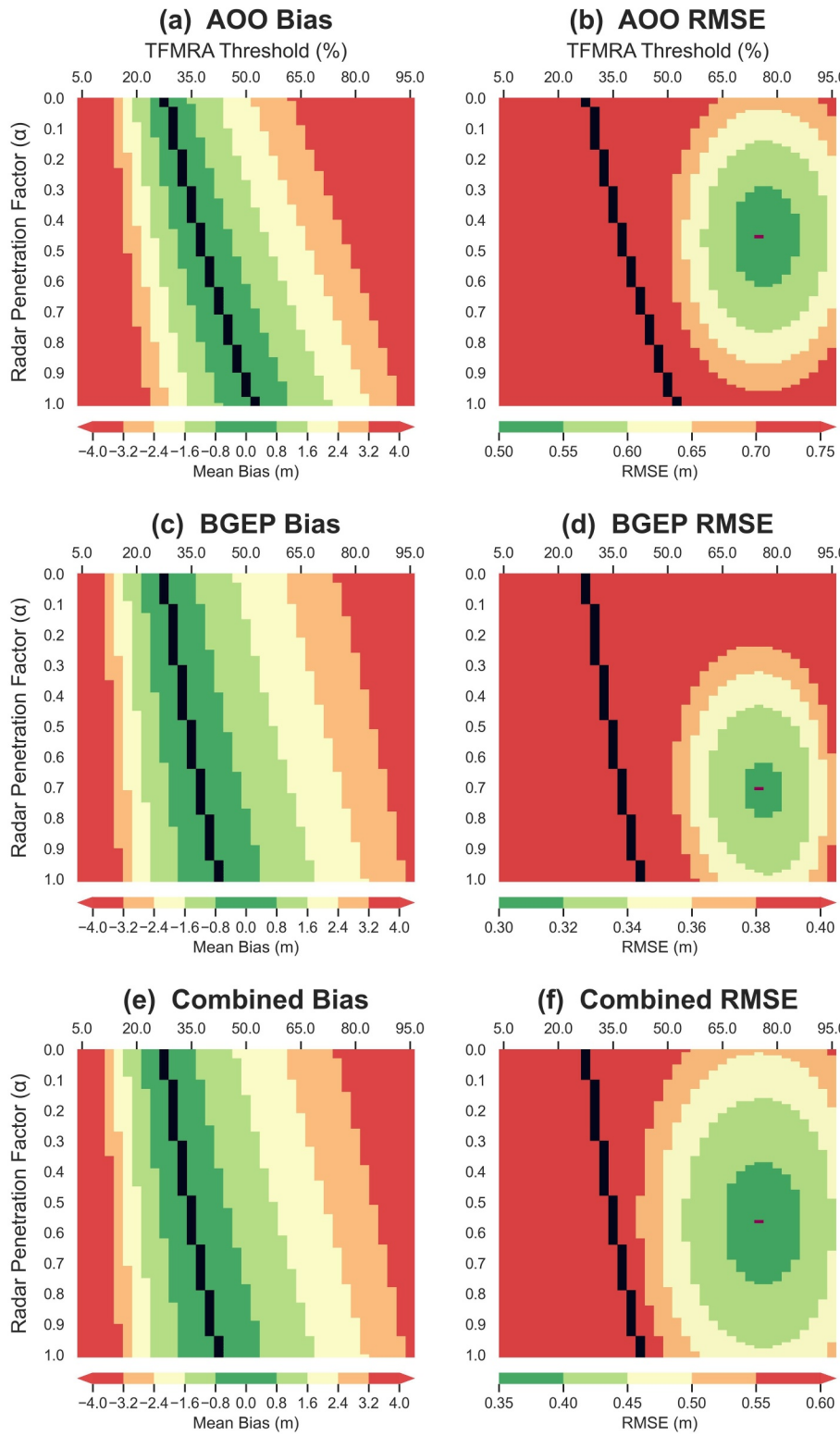

Figure 2. Mean bias (left) and RMSE (right) between anomalies of sea ice thickness derived from CS2 and at the moorings, at incremental values of assumed radar penetration and retracking threshold. Top row shows AAO moorings ($n = 63$), middle row shows BGEP moorings ($n = 216$), bottom row shows all moorings ($n = 279$). Black line shows the threshold value where bias is minimized for a given α value. The combination of assumed radar penetration and retracking threshold at which the RMSE is minimized is shown in purple.

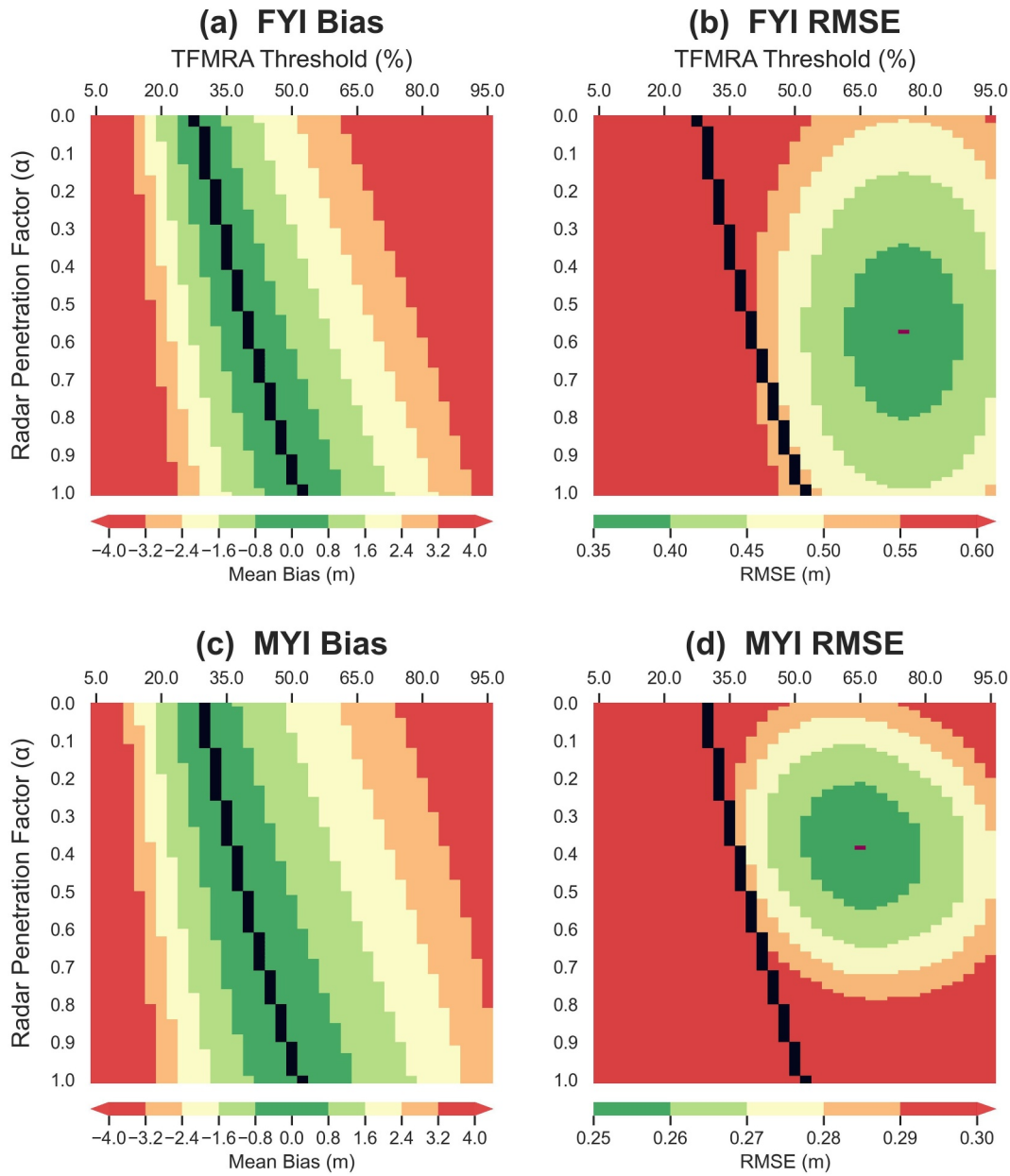

Figure 3. Mean bias (left) and RMSE (right) between anomalies of sea ice thickness derived from CS2 and at the moorings, at incremental values of assumed radar penetration and retracking threshold. Top row shows FYI ($n = 214$), bottom row shows MYI ($n = 65$). Black line shows the threshold value where bias is minimized for a given α value. The combination of assumed radar penetration and retracking threshold at which the RMSE is minimized is shown in purple.

Modeling studies have previously suggested that radar penetration is higher over MYI than FYI, due to a lack of salty brine in the snow overlying MYI (Nandan et al., 2017, 2020). However, our results imply the opposite, with lower optimal α values calculated over MYI. We suggest two possible reasons for this: The first may be that volume scattering (as opposed to surface scattering) may become more significant in the deeper and potentially coarser-grained snowpacks associated with MYI, reducing backscatter from the ice surface while backscatter from the snow surface remains the same. The second (and potentially much more significant) reason is increased roughness (decreased specularity) associated with MYI, leading to fewer coherent returns from the ice surface relative to the snow surface (De Rijke-Thomas et al., 2023). When analyzing CryoSat-2's SARin mode, De Rijke-Thomas et al. (2023, Figure 11) found a higher degree of coherence for FYI returns.

The higher interannual skill at α <1 suggests that the real, mean height of backscattered power corresponds to neither the mean ice surface nor the mean snow surface. However, Figure 3 also indicates that the degree to which this is the case depends on the ice type.

We find a small sensitivity in the optimal α to the snow depth and bulk sea density used in the SIT calculation. When increasing the snow depth used in our SIT calculations by 10%, we find a small decrease in the number of α/threshold combinations in the lowest RMSE class (Figure S9 in Supporting Information S1). When decreasing the snow depth by 10%, we find no noticeable difference in our results (Figure S10 in Supporting Information S1). When using the output of SM-LG forced by MERRA-2, we find a consistent increase in RMSE of 0.01 m at the BGEP moorings (Figure S11 in Supporting Information S1). At the AOO moorings, no clear change is perceivable. When increasing our bulk sea ice densities by 1.3% (FYI) and 2.3% (MYI), as per Jutila, Hendricks, et al. (2022), we find an increase in RMSE of 0.02–0.04 m at all of the moorings (Figure S12 in Supporting Information S1). We find no change in the combination of assumed radar penetration and retracking threshold at which the RMSE is minimized (shown in purple) when changing these parameters. For each of the snow depth and sea ice bulk density values tested, the threshold/α combination at which the RMSE is minimized is at thresholds of 70%–85% and $0.4 < \alpha < 0.8$, when the moorings are combined.

4.2. Optimal Combination of Threshold and α

Our results suggest an optimal retracking threshold of 70%–85% and $0.4 < \alpha < 0.8$ when investigating interannual trends in sea ice thickness. However, there appears to be no 'perfect' combination of threshold and α: At our optimal values for α, there is generally a bias of >2.5 m, and at our optimal thresholds the skill in representing interannual variability is reduced or not statistically significant. This suggests the need for a compromise between the two metrics, with the α and threshold values chosen as a combination where the two are both optimized as much as possible. For example, our results show that at α >0.6, there is still some skill in representing interannual variability at thresholds of 45%–55%, at which the bias is also minimal (<0.8 m).

Our results suggest sea ice thickness products could be optimized for their purpose: When aiming to analyze interannual variability, the skill of the product should be maximized (dark green areas on the RMSE plots), with a correction for any induced bias applied. When analyzing absolute values, the bias should be minimized (dark green areas on the bias plots), with less attention paid to the skill of the product in representing interannual variability.

Correction for bias in the SIT processing chain is common. For example, in the standard CPOM and AWI SIT processing chains for CryoSat's SAR mode, fixed bias corrections of −16.26 cm and −4.7 cm are applied, respectively (Hendricks et al., 2024; Tilling et al., 2018). In the CPOM processing chain, this correction is applied to elevation estimates from leads and the sea ice surface, to account for the different methods used to retrack leads (Giles et al., 2007) and floes (Tilling et al., 2018). In the AWI processing chain, the bias correction is applied to all elevation estimates (Hendricks et al., 2024). We note that the purpose of these two corrections differs: In the CPOM processing chain, it is applied to correct for a retracker bias between surfaces, whilst in the AWI processing chain it is applied to correct for range biases between different radar modes. To consolidate our optimal α and threshold results, a similar fixed threshold-dependent bias correction could be calculated to align the black minimal bias line shown on Figure 2e with the dark green RMSE area on Figure 2f. Over FYI and MYI, a positive bias correction would need to be applied to the radar freeboards on the order of 20 cm, as errors in the freeboard increase roughly ten-fold in the freeboard-to-thickness conversion (Ricker et al., 2014). As bias correction is already ubiquitous, we argue that the skills of SIT products could be effectively improved by first tuning the α and retracking threshold to maximimise interannual variability, before applying bias correction to retrieve the correct absolute SIT values.

Our results suggest that, over MYI, the use of a lower retracking threshold is more effective, assuming lower α values, than over FYI. This is supported by Ricker et al. (2014), who suggested that in "scenarios where the main scattering horizon is not penetrating the snow load completely, the usage of a low-threshold retracker might be reasonable". Additionally, these results are consistent with the Lognormal Altimeter Retracker Model (LARM; Landy et al., 2020), a physical retracker that decreases the percentage threshold with increasing large-scale sea ice roughness. Our results also support the possibility of seasonal/regional retrackers to maximize skill, as suggested by Ricker et al. (2014).

4.3. Implications and Future Directions

The scarcity of independent in situ sea ice thickness data means that this analysis is currently limited to the Beaufort Sea and Fram Strait. However, the magnitude of our derived α values is consistent with those of Nab et al. (Figures 2, 2023), who calculated $0.4 < \alpha < 0.8$. However, we find a significant ice type dependence which was not observed in the previous work.

To support the results of our optimization approach, we estimate the CryoSat-2 ice freeboard error as a function of Operation IceBridge (OIB) snow depth (Section 2 in Supporting Information S1), finding $0.4 < \alpha < 0.8$ in March–April (2011–2018) depending on the snow depth product used. These findings suggest our α is representative of the mean α values found in regions outside the Beaufort Sea and Fram Strait. The OIB-derived α values' high dependence on the snow depth product used, in contrast to our main analysis' small sensitivity to the snow depth product used (Section 4.1) shows the benefit of conducting this analysis using the ULS moorings.

Our method of deriving optimal α/TFMRA-combination values has several potential applications: The most obvious is its use in future CryoSat-2 radar freeboard-to-thickness processing chains to generate more skillful retrievals. We also point out that this technique can be used for any satellite radar-altimetry mission with a sufficiently long timeseries such that a climatology can be generated. We therefore anticipate the use of this technique on radar freeboards from the SARAL/AltiKa mission (Armitage & Ridout, 2015). Ultimately, our results pave the way for 'partial penetration' sea ice thickness products from both Ku- and Ka-band radar altimetry missions.

The extraction of appropriate α values for CryoSat-2 may also facilitate more skillful retrieval of snow depths from dual-frequency altimetry with either ICESat-2 (Kacimi & Kwok, 2022) or SARAL/AltiKa (e.g., Guerreiro et al., 2016). Reducing the α values without changing the TFMRA-thresholds would increase the retrieved snow depths and may address the apparent low bias in the dual-frequency retrievals of Garnier et al. (2021). The European Space Agency is currently planning a new, dual-frequency altimetry mission for the cryosphere (CRISTAL; M. Kern et al., 2020). This is anticipated to launch in early 2028, and aims to retrieve snow depths through differential penetration of returned radar waves in the Ku- and Ka-bands. Our findings of incomplete penetration imply that a considerable calibration exercise (e.g., following Lawrence et al., 2018) will be required to retrieve snow depths in line with observations.

Finally, we highlight that an effort is currently underway to inter-compare a variety of sea ice thickness products from satellites (SIN'XS; https://sinxs.noveltis.fr). We suggest that calculating sea ice thickness under the assumption of partial-penetration stands to improve the skill of these products at capturing interannual variability. In addition, the rubric for assessment of a product's skill should be given careful consideration.

Data Availability Statement

All code required to reproduce this analysis can be found at Nab (2024). The BGEP mooring data can be found at BGEP (2022). The AOO mooring data can be found at Sumata (2022). The ice type data can be found at Aaboe et al. (2021). The SM-LG snow depth and density data can be found at Liston et al. (2021). The pysiral code can be found at Hendricks et al. (2024). The along-track CS2 waveforms can be found at European Space Agency (2019). The monthly sea ice thickness products from the GSFC, CPOM and AWI can be found at Kurtz and Harbeck (2017), Tilling et al. (2018) and Hendricks and Paul (2023) respectively. The OIB Quick-Look and snow radar data can be found at Kurtz et al. (2016) and Paden et al. (2014) respectively. The pySnowRadar code can be found at King et al. (2020).

Acknowledgments
CJN and CAJN acknowledge support from NERC (#NE/S007229/1). CJN also acknowledges support from the UK Met Office (CASE Partnership). JS acknowledges support from the Canada 150 Chair Program (C150; #50296) and Horizon 2020 (#101003826). RM acknowledges support NERC (#NE/L002485/1) and the C150 via JS. MT acknowledges support from ESA (#ESA/AO/1–9132/17/NL/MP, #ESA/AO/1-11448/22/I-AG, #ESA/AO/1–10061/19/I-EF, and SIN'XS) and NERC (#NE/T000546/1 and #NE/X004643/1). RM acknowledges support from the International Space Science Institute (ISSI), through ISSI International Team project #510. The authors would like to thank Stefan Hendricks for his insight and constructive feedback on the analysis. CJN would also like to thank the Earth Observation Group at UiT for hosting her during the production of this manuscript.

References

Aaboe, S., Down, E., Sørensen, A., Lavergne, T., & Eastwood, S. (2021). Sea-ice type climate data record Oct 1978-Aug 2023 Version 2.0. *Copernicus Climate Change Service (C3S) Climate Data Store (CDS)*. [Dataset]. ECMWF. https://doi.org/10.24381/CDS.29C46D83

Alexandrov, V., Sandven, S., Wahlin, J., & Johannessen, O. M. (2010). The relation between sea ice thickness and freeboard in the Arctic. *The Cryosphere*, *4*(3), 373–380. https://doi.org/10.5194/tc-4-373-2010

Armitage, T. W. K., & Ridout, A. L. (2015). Arctic sea ice freeboard from AltiKa and comparison with CryoSat-2 and operation IceBridge. *Geophysical Research Letters*, *42*(16), 6724–6731. https://doi.org/10.1002/2015GL064823

BGEP. (2022). Mooring data from the Beaufort gyre exploration project (BGEP). [Dataset]. Retrieved from https://www2.whoi.edu/site/beaufortgyre/data/mooring-data/

Bocquet, M., Fleury, S., Piras, F., Rinne, E., Sallila, H., Garnier, F., & Rémy, F. (2023). Arctic sea ice radar freeboard retrieval from the European remote-sensing satellite (ERS-2) using altimetry: Toward sea ice thickness observation from 1995 to 2021. *The Cryosphere*, *17*(7), 3013–3039. https://doi.org/10.5194/tc-17-3013-2023

De Rijke-Thomas, C., Landy, J. C., Mallett, R., Willatt, R. C., Tsamados, M., & King, J. (2023). Airborne investigation of quasi-specular ku-band radar scattering for satellite altimetry over snow-covered Arctic sea ice. *IEEE Transactions on Geoscience and Remote Sensing*, *61*, 1–19. https://doi.org/10.1109/TGRS.2023.3318263

European Space Agency. (2019). Cryosat L1b SAR precise orbit. Baseline D. *Institution: European Space Agency*. [Dataset]. https://doi.org/10.5270/CR2-2cnblvi

Garnier, F., Fleury, S., Garric, G., Bouffard, J., Tsamados, M., Laforge, A., et al. (2021). Advances in altimetric snow depth estimates using bi-frequency SARAL and CryoSat-2 Ka–Ku measurements. *The Cryosphere*, *15*(12), 5483–5512. https://doi.org/10.5194/tc-15-5483-2021

Giles, K., Laxon, S. W., Wingham, D., Wallis, D., Krabill, W., Leuschen, C., et al. (2007). Combined airborne laser and radar altimeter measurements over the Fram Strait in May 2002. *Remote Sensing of Environment*, *111*(2–3), 182–194. https://doi.org/10.1016/j.rse.2007.02.037

Guerreiro, K., Fleury, S., Zakharova, E., Kouraev, A., Rémy, F., & Maisongrande, P. (2017). Comparison of CryoSat-2 and ENVISAT radar freeboard over Arctic sea ice: Toward an improved envisat freeboard retrieval. *The Cryosphere*, *11*(5), 2059–2073. https://doi.org/10.5194/tc-11-2059-2017

Guerreiro, K., Fleury, S., Zakharova, E., Rémy, F., & Kouraev, A. (2016). Potential for estimation of snow depth on Arctic sea ice from CryoSat-2 and SARAL/AltiKa missions. *Remote Sensing of Environment*, *186*, 339–349. https://doi.org/10.1016/j.rse.2016.07.013

Hendricks, S., Brockley, D., Paul, S., & Sallila, H. (2024). python sea ice radar altimetry toolbox (version 0.11). https://doi.org/10.5281/ZENODO.5566346

Hendricks, S., & Paul, S. (2023). Product user guide and algorithm specification: AWI CryoSat-2 sea ice thickness (version 2.6). https://doi.org/10.5281/zenodo.10044554

Howell, S. E. L., Babb, D. G., Landy, J. C., Glissenaar, I. A., McNeil, K., Montpetit, B., & Brady, M. (2024). Sea ice transport and replenishment across and within the Canadian Arctic Archipelago, 2016–2022. *The Cryosphere*, *18*(5), 2321–2333. https://doi.org/10.5194/tc-18-2321-2024

Jiang, M., Zhong, W., Xu, K., & Jia, Y. (2023). Estimation of Arctic sea ice thickness from Chinese HY-2B radar altimetry data. *Remote Sensing*, *15*(5), 1180. https://doi.org/10.3390/rs15051180

Jutila, A., Hendricks, S., Ricker, R., von Albedyll, L., Krumpen, T., & Haas, C. (2022a). Retrieval and parameterisation of sea-ice bulk density from airborne multi-sensor measurements. *The Cryosphere*, *16*(1), 259–275. https://doi.org/10.5194/tc-16-259-2022

Kacimi, S., & Kwok, R. (2022). Arctic snow depth, ice thickness, and volume from ICESat-2 and CryoSat-2: 2018–2021. *Geophysical Research Letters*, *49*(5), e2021GL097448. https://doi.org/10.1029/2021GL097448

Kern, M., Cullen, R., Berruti, B., Bouffard, J., Casal, T., Drinkwater, M. R., et al. (2020). The copernicus polar ice and snow topography altimeter (CRISTAL) high-priority candidate mission. *The Cryosphere*, *14*(7), 2235–2251. https://doi.org/10.5194/tc-14-2235-2020

Kern, S., Khvorostovsky, K., Skourup, H., Rinne, E., Parsakhoo, Z. S., Djepa, V., et al. (2015). The impact of snow depth, snow density and ice density on sea ice thickness retrieval from satellite radar altimetry: Results from the ESA-CCI sea ice ECV project round robin exercise. *The Cryosphere*, *9*(1), 37–52. https://doi.org/10.5194/tc-9-37-2015

King, J., Brady, M., & Newman, T. (2020). kingjml/pySnowRadar: Updated IEEE TGRS Submission. https://doi.org/10.5281/ZENODO.4071947

King, J., Skourup, H., Hvidegaard, S. M., Rösel, A., Gerland, S., Spreen, G., et al. (2018). Comparison of freeboard retrieval and ice thickness calculation from ALS, ASIRAS, and CryoSat-2 in the Norwegian arctic to field measurements made during the N-ICE2015 expedition. *Journal of Geophysical Research: Oceans*, *123*(2), 1123–1141. https://doi.org/10.1002/2017JC013233

Kurtz, N. T., Galin, N., & Studinger, M. (2014). An improved CryoSat-2 sea ice freeboard retrieval algorithm through the use of waveform fitting. *The Cryosphere*, *8*(4), 1217–1237. https://doi.org/10.5194/tc-8-1217-2014

Kurtz, N. T., & Harbeck, J. (2017). CryoSat-2 level 4 sea ice elevation, freeboard, and thickness. (RDEFT4, Version 1). [Dataset]. *NASA National Snow and Ice Data Center Distributed Active Archive Center*. https://doi.org/10.5067/96JO0KIFDAS8

Kurtz, N. T., Studinger, M., Harbeck, J., Onana, V., & Yi, D. (2016). IceBridge Sea Ice Freeboard, Snow Depth, and Thickness Quick Look. (NSIDC-0708, Version 1). [Dataset]. https://doi.org/10.5067/GRIXZ91DE0L9

Kwok, R. (2018). Arctic sea ice thickness, volume, and multiyear ice coverage: Losses and coupled variability (1958–2018). *Environmental Research Letters*, *13*(10), 105005. https://doi.org/10.1088/1748-9326/aae3ec

Kwok, R., & Cunningham, G. F. (2015). Variability of Arctic sea ice thickness and volume from CryoSat-2. *Philosophical Transactions of the Royal Society A: Mathematical, Physical & Engineering Sciences*, *373*(2045), 20140157. https://doi.org/10.1098/rsta.2014.0157

Landy, J. C., Petty, A. A., Tsamados, M., & Stroeve, J. C. (2020). Sea ice roughness overlooked as a key source of uncertainty in CryoSat-2 ice freeboard retrievals. *Journal of Geophysical Research: Oceans*, *125*(5). https://doi.org/10.1029/2019JC015820

Lawrence, I. R. (2019). *Multi-satellite synergies for polar ocean altimetry (PhD)*. University.

Lawrence, I. R., Tsamados, M. C., Stroeve, J. C., Armitage, T. W. K., & Ridout, A. L. (2018). Estimating snow depth over Arctic sea ice from calibrated dual-frequency radar freeboards. *The Cryosphere*, *12*(11), 3551–3564. https://doi.org/10.5194/tc-12-3551-2018

Laxon, S. W., Giles, K. A., Ridout, A. L., Wingham, D. J., Willatt, R., Cullen, R., et al. (2013). CryoSat-2 estimates of Arctic sea ice thickness and volume. *Geophysical Research Letters*, *40*(4), 732–737. https://doi.org/10.1002/grl.50193

Laxon, S. W., Peacock, N., & Smith, D. (2003). High interannual variability of sea ice thickness in the Arctic region. *Nature*, *425*(6961), 947–950. https://doi.org/10.1038/nature02050

Liston, G., Itkin, P., Stroeve, J., Tschudi, M., Stewart, J. S., Pedersen, S. H., et al. (2020). A Lagrangian snow-evolution system for sea-ice applications (SnowModel-LG): Part I—Model description. *Journal of Geophysical Research: Oceans*, *125*(10). https://doi.org/10.1029/2019JC015913

Liston, G., Stroeve, J., & Itkin, P. (2021). Lagrangian snow distributions for sea-ice applications. ERA5 subset. *NASA National Snow and Ice Data Center Distributed Active Archive Center*. [Dataset]. https://doi.org/10.5067/27A0P5M6LZBI

Nab, C. (2024). carmennab/cs2_skill: V1. *Zenodo*. [software]. https://doi.org/10.5281/ZENODO.13762641

Nab, C., Mallett, R., Gregory, W., Landy, J., Lawrence, I. R., Willatt, R., et al. (2023). Synoptic variability in satellite altimeter-derived radar freeboard of Arctic sea ice. *Geophysical Research Letters*, *50*(2). https://doi.org/10.1029/2022GL100696

Nandan, V., Geldsetzer, T., Yackel, J., Mahmud, M., Scharien, R., Howell, S., et al. (2017). Effect of snow salinity on CryoSat-2 arctic first-year sea ice freeboard measurements: Sea ice brine-snow effect on CryoSat-2. *Geophysical Research Letters*, *44*(20), 10419–10426. https://doi.org/10.1002/2017GL074506

Nandan, V., Scharien, R. K., Geldsetzer, T., Kwok, R., Yackel, J. J., Mahmud, M. S., et al. (2020). Snow property controls on modeled ku-band altimeter estimates of first-year sea ice thickness: Case studies from the Canadian and Norwegian arctic. *Ieee Journal of Selected Topics in Applied Earth Observations and Remote Sensing*, *13*, 1082–1096. https://doi.org/10.1109/JSTARS.2020.2966432

OSI SAF. (2022). GBL AMSR SICO CDR R3Global sea ice concentration climate data record v3.0 (AMSR) - multimission. *OSI SAF*. https://doi.org/10.15770/EUM_SAF_OSI_0015

Paden, J., Li, Leuschen, C., & Rodriguez-Morales, F., & Hale. (2014). IceBridge snow radar L1B geolocated radar echo strength profiles Version 2 [Dataset]. https://doi.org/10.5067/FAZTWP500V70

Rantanen, M., Karpechko, A. Y., Lipponen, A., Nordling, K., Hyvärinen, O., Ruosteenoja, K., et al. (2022). The Arctic has warmed nearly four times faster than the globe since 1979. *Communications Earth & Environment*, *3*(1), 168. https://doi.org/10.1038/s43247-022-00498-3

Ricker, R., Hendricks, S., Helm, V., Skourup, H., & Davidson, M. (2014). Sensitivity of CryoSat-2 Arctic sea-ice freeboard and thickness on radar-waveform interpretation. *The Cryosphere*, *8*(4), 1607–1622. https://doi.org/10.5194/tc-8-1607-2014

Ricker, R., Hendricks, S., Kaleschke, L., Tian-Kunze, X., King, J., & Haas, C. (2017). A weekly Arctic sea-ice thickness data record from merged CryoSat-2 and SMOS satellite data. *The Cryosphere*, *11*(4), 1607–1623. https://doi.org/10.5194/tc-11-1607-2017

Ricker, R., Hendricks, S., Perovich, D. K., Helm, V., & Gerdes, R. (2015). Impact of snow accumulation on CryoSat-2 range retrievals over Arctic sea ice: An observational approach with buoy data. *Geophysical Research Letters*, *42*(11), 4447–4455. https://doi.org/10.1002/2015GL064081

Stroeve, J., & Notz, D. (2018). Changing state of Arctic sea ice across all seasons. *Environmental Research Letters*, *13*(10), 103001. https://doi.org/10.1088/1748-9326/aade56

Stroeve, J., Veyssiere, G., Nab, C., Light, B., Perovich, D., Laliberté, J., et al. (2024). Mapping potential timing of ice algal blooms from satellite. *Geophysical Research Letters*, *51*(8), e2023GL106486. https://doi.org/10.1029/2023GL106486

Sumata, H. (2022). Monthly sea ice thickness distribution in Fram Strait. [Dataset]. https://doi.org/10.21334/NPOLAR.2022.B94CB848

Sumata, H., De Steur, L., Gerland, S., Divine, D. V., & Pavlova, O. (2022). Unprecedented decline of Arctic sea ice outflow in 2018. *Nature Communications*, *13*(1), 1747. https://doi.org/10.1038/s41467-022-29470-7

Tilling, R. L. (2016). *New observations of Arctic sea ice from satellite radar altimetry (PhD)*. University.

Tilling, R. L., Ridout, A., & Shepherd, A. (2018). Estimating Arctic sea ice thickness and volume using CryoSat-2 radar altimeter data. *Advances in Space Research*, *62*(6), 1203–1225. https://doi.org/10.1016/j.asr.2017.10.051

Willatt, R., Giles, K., Laxon, S. W., Stone-Drake, L., & Worby, A. (2010). Field investigations of ku-band radar penetration into snow cover on antarctic sea ice. *IEEE Transactions on Geoscience and Remote Sensing*, *48*(1), 365–372. https://doi.org/10.1109/TGRS.2009.2028237

Willatt, R., Laxon, S. W., Giles, K., Cullen, R., Haas, C., & Helm, V. (2011). Ku-band radar penetration into snow cover on Arctic sea ice using airborne data. *Annals of Glaciology*, *52*(57), 197–205. https://doi.org/10.3189/172756411795931589

Willatt, R., Stroeve, J. C., Nandan, V., Newman, T., Mallett, R., Hendricks, S., et al. (2023). Retrieval of snow depth on Arctic sea ice from surface-based, polarimetric, dual-frequency radar altimetry. *Geophysical Research Letters*, *50*(20), e2023GL104461. https://doi.org/10.1029/2023GL104461

References From the Supporting Information

Fetterer, F. M., Knowles, K., Meier, W., Savoie, M., & Windnagel, A. (2017). Sea ice index Version 3 [Dataset]. *NSIDC*. https://doi.org/10.7265/N5K072F8

Gregory, W., Lawrence, I. R., & Tsamados, M. (2021). A Bayesian approach towards daily pan-Arctic sea ice freeboard estimates from combined CryoSat-2 and Sentinel-3 satellite observations. *The Cryosphere*, *15*(6), 2857–2871. https://doi.org/10.5194/tc-15-2857-2021

Jutila, A., King, J., Paden, J., Ricker, R., Hendricks, S., Polashenski, C., et al. (2022b). High-resolution snow depth on Arctic sea ice from low-altitude airborne microwave radar data. *IEEE Transactions on Geoscience and Remote Sensing*, *60*, 1–16. https://doi.org/10.1109/TGRS.2021.3063756

Krabill, W. B. (2013). IceBridge ATM L1B elevation and return strength. (Version 2). *NASA National Snow and Ice Data Center DAAC*. https://doi.org/10.5067/19SIM5TXKPGT

Krabill, W. B., Thomas, R. H., Martin, C. F., Swift, R. N., & Frederick, E. B. (1995). Accuracy of airborne laser altimetry over the Greenland ice sheet. *International Journal of Remote Sensing*, *16*(7), 1211–1222. https://doi.org/10.1080/01431169508954472

Kwok, R., Kurtz, N. T., Brucker, L., Ivanoff, A., Newman, T., Farrell, S. L., et al. (2017). Intercomparison of snow depth retrievals over Arctic sea ice from radar data acquired by Operation IceBridge. *The Cryosphere*, *11*(6), 2571–2593. https://doi.org/10.5194/tc-11-2571-2017

Newman, T., Farrell, S. L., Richter-Menge, J., Connor, L. N., Kurtz, N. T., Elder, B. C., & McAdoo, D. (2014). Assessment of radar-derived snow depth over Arctic sea ice. *Journal of Geophysical Research: Oceans*, *119*(12), 8578–8602. https://doi.org/10.1002/2014JC010284